euspen's 25th International Conference & Exhibition, Zaragoza, ES, June 2025
www.euspen.eu

Quality improvement of laser-microstructured riblet geometries in forming tools for enhanced efficiency of injection-moulded fan impellers

Daniel Gitzel[1], Eric Gärtner[1], Mikel Lucas Garcia de Albeniz[2], Jan Edelmann[1], Peter Leitl[2]

[1]*Fraunhofer IWU Institute for Machine Tools and Forming Technology, Chemnitz, Germany*
[2]*Bionic Surface Technologies, Graz, Austria*

daniel.gitzel@iwu.fraunhofer.de

Abstract
With the aim of reducing air resistance and thus increasing the efficiency of industrial fans, this study investigates high-rate laser functionalization of complex 3D surfaces to integrate tailored riblets. It focuses on laser micromachining V-grooves into moulding tools to create microstructures on fan impeller surfaces. The riblets with spacings of 100 µm to 300 µm and depths of 50 µm to 150 µm are designed to optimise the air flow. Research shows that nano- and micro-structured surfaces, mimicking shark skin, significantly decrease air resistance and energy consumption, especially for 3D streamlined bodies, positively affecting flow separation. By varying the size and shape of the riblets, different effects can be achieved on the textured surface. However, the design and application of riblets on rapidly rotating parts such as fan wheels is still a major challenge today. Ideally, riblet dimensions should change stepless according to the object's geometry, but common adhesive foils including the riblet coating do not meet this requirement. To overcome this challenge, microstructures were fabricated using direct laser writing with ultra-short pulsed laser radiation operating at a wavelength of 1030 nm on the mould. The primary objective of this research was to optimize the surface and shape quality of these microstructures by minimizing roughness, burr, and spatter occurrence. To achieve this, the laser fluence was systematically investigated and the effects of different pulse and line spacings were analysed. Results were quantitatively assessed through measurements of surface roughness, as well as ablated volume per energy and time, which indicate the efficiency and productivity of the laser process. These findings enhance industrial fan production and provide insights into optimizing laser-based microstructuring processes for surface functionalization.

Keywords: Injection, Laser micro machining, Resistance, Fan Impeller

1. Introduction

Industrial fans are used in a wide range of applications and their main function is to provide a stable and continuous flow of air. Given that these fans normally operate with a continuous massflow, the increase of efficiency will be achieved mainly through a lower power consumption. Different parameters are involved in the power consumption of a fan like this, but one of high interest is the drag of the blade with the fluid.

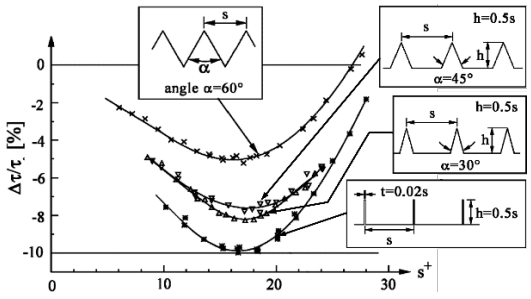

Figure 1. Drag reduction curve for different riblet geometries [1]

Therefore, the riblet technology was chosen for this project. Riblets are microstructures that resemble features of the shark skin. When they are properly designed riblets can lead to a significant reduction of the viscous drag [2]. Figure 1 shows the different achievable drag reduction considering the geometry of the riblets [1]. On the one hand, it can be seen a maximal drag reduction of 10 % when blade riblets are used. They present major production challenges, and its mechanical stability is very compromised. On the other hand, the most stable structure is the sawtooth offering up to 6 % of drag reduction. As a compromise trapezoidal riblets were applied, as they offer up to 8 % drag reduction and sufficient mechanical properties.

2. Design and simulation of riblet geometries

Even though riblet technology has been known for several years their correct design is a complicated endeavour. The best riblet geometry and positioning could be characterized, due to the developed algorithm and numerical simulations by [3].

The geometry of the fan was facilitated by [4]. After a mesh independency study, it was concluded that a numerical discretization of the fluid to be simulated made of tetrahedral elements was the best compromise between computational time and accuracy of the Computational Fluid Dynamics calculations. Moreover, for the riblet simulations, it is necessary to discretize in detail the boundary layer (region of fluid close to the wall), and this is why this region was discretized with prism layers. A very thin prism layer discretization that resolves the viscous sublayer of the turbulent boundary layer was done. This was necessary because in order to have a precise riblet design the viscous sub-layer must be resolved. Also, a periodic domain of 90° was chosen to reduce the computational cost of the simulations given as a result a mesh with roughly 14 million cells.

The boundary conditions of the simulations are summarized in Table 1. In this case, different operating points of the fan were established and one of them, the so-called Design Point (DP), was chosen as the reference for the riblet design.

Table 1 Boundary conditions at DP for the simulation

Air density	[kg/m³]	1.187
Air viscosity	[Pa s]	18.13 e-6
Reference pressure	[Pa]	101325
Rotational speed	[rpm]	941
Volume flow	[m³/h]	9077

All numerical simulations were implemented using the commercial finite-volume software CFX®, which is developed by ANSYS®. Considering the characteristics of the system a steady-state approach was chosen and the turbulence model selected for these simulations was the SST-k-ω [5].

Figure 2 shows the wall-shear distribution on both Pressure Side (PS) and Suction Side (SS) of the fan's blades (spots where the riblets will be applied). With these information and values of torque and pressure along the domain the simulation was validated and consequently used for the riblet design.

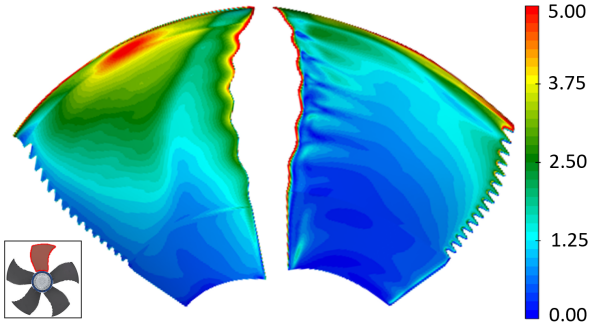

Figure 2. Wall shear stress distribution expressed in Pascal on SS (left) and PS (right). Fan impeller image based on [4].

The already validated simulation was used as a reference by the algorithm to calculate the ideal riblet size and their orientation. As the flow conditions vary across the surface, the size was discretized to maximise the potential of the riblets. Therefore, the riblet geometry differs in its size. A tip-to-tip distance of 300 µm and a riblet height of 150 µm were chosen as a representative of these simulation results for the development of the laser process.

The riblet algorithm also predicted the impact of riblets on the surface of the fan. The relative improvement of efficiency was analysed depending on the surface roughness. Three simulations were performed, one with a rough surface (Ra = 2.24 µm based on VDI 3400 surface class 27 [6]), one with hydrodynamically smooth surface (Ra approx. 0 µm) and one with the riblet distribution on it. As the results in Table 2 show, the hydrodynamically smooth surface already has a positive effect, which is further enhanced by the use of riblets.

Table 2 Relative efficiency of the fan in the operating point for 3 different surfaces

Surface	Rough	Smooth	Ideal riblets
Δ Efficiency [%]	reference	0,123	2,209

3. Material, experimental setup and methods

The laser microstructures were fabricated on high-alloy hot-work tool steel 1.2343 ESU which is well established for injection moulding applications due to his good polishing properties. The initial workpiece surface was grinded to produce a homogeneous surface with low roughness. Due to the pre grinding process, the moulds exhibited a significant directional roughness of approximately Sa = 0.33 µm.

It should be noted that when manufacturing industrial fans by injection moulding, the profile on the mould insert is the opposite of the profile that is to be obtained in the final product. This means that V-grooves must be machined using the laser micromachining to create riblets on the fan impeller.

Regarding the shape of the riblets, the following boundary conditions must be considered during structuring, otherwise the functionality of the riblets may be negatively affected. The tip is expected to be rounded due to the manufacturing process. But the sharpness of the tip is important. The aim for the laser process is to keep the rounding as low as possible, considering the structuring time. In addition, scalability of the riblet geometry must be ensured. This means that the ratio of rounding radius to tip-to-tip-distance must remain constant. If this is not the case, it could lead to the contour of the riblets being lost.

A femtosecond laser source (TruMicro 2030, P_{AV} = 20 W) was used for the experiments. The laser beam was circular polarized by a λ/4-plate and directed through two mirrors and a beam expander with two lenses onto the galvanometer scanner (ExcelliScan 14). An f-theta objective with a focal length of 100 mm focused the beam to a spot diameter ($1/e^2$) $2w_0$ = 16.9 µm in the working plane. To analyse the removal rate and roughness, 2 x 2 mm² square hollows were produced. V-grooves according to the riblet design (see section 2.) with tip-to-tip distance s = 300 µm, height h = 150 µm and wall angle α = 40° were fabricated to evaluate the laser micro structuring process of trapezoidal riblets.

The repetition rate was set to f_{rep} = 200 kHz. Unless otherwise stated for variation tests, the pulse duration was τ = 0.35 ps, the scanning speed v_{Mark} = 1 m/s, the line distance Ld = 5 µm and the number of passes N = 100 by bidirectional scanning. Cleaned compressed air was blown horizontally over the sample at 3 bar from a nozzle (outlet size 25 x 2 mm²) to prevent debris from depositing in the processing area. The crossjet was exhausted on the opposite side. After laser processing, the samples were cleaned for 60 minutes with ethanol in an ultrasonic bath.

The grinded surface of the mould and the laser structured sample surfaces were measured using a confocal microscope MarSurf CM mobile (Co. Mahr) and analysed in MountainsMap (Co. Digital Surf). For the evaluation of the surface roughness parameters according to DIN EN ISO 25178-2 an area with the size of 1.6 mm x 1.6 mm was measured and filtered with a Gaussian filter according to DIN EN ISO 25178-3 with a cut off wavelength of λc = 0.8 mm and λs = 0.0025 mm.

4. Laser process development for riblet machining

4.1. Pulse duration

To determine the influence of the pulse duration on the ablation rate and surface roughness, pulse durations from τ = 350 fs to τ = 20 ps were selected. The experiments were carried out without hatch rotation. The surface roughness and the ablation rate as a function of the pulse duration are depicted in Figure 3.

The ablation rate increases as the pulse duration decreases. This is due to the fact that the same amount of energy is applied in a shorter time with a shorter pulse duration. The electrons have less time to transfer the energy to the phonon system. As a result, less energy is converted into heat, but more energy flows into the direct vaporization of the material [7]. As a result, the proportion of vaporization increases and the energy specific volume $\Delta V/\Delta E$ rises. Conversely, the surface roughness increases with decreasing pulse duration from τ = 20 ps to τ = 3 ps due to evaporation and the laser induced plasma. As the pulse duration increases, the proportion of melt in the ablation increases, which leads to a remelting effect and a lower surface roughness. For precision laser micro machining, the pulse

duration should be shorter than the electron-phonon relaxation time [7], as the roughness subsequently decreases again.

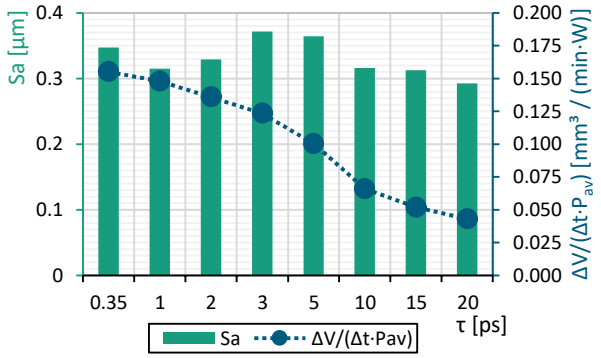

Figure 3. Arithmetical mean height Sa and energy specific volume ΔV/(Δt·Pav) as a function of pulse duration

The benefit of the increased removal rate and the resulting shorter process time is more important in this application than the increase in surface roughness. Since the change in surface roughness in this dimension has no significant influence on the riblet impact (see section 2), the decision was made to use femtosecond laser pulses.

4.2. Pulse and line distance

To evaluate the impact of pulse distance (Pd) and line distance (Ld) to riblet machining, a test plan was set up, as shown in Table 3. Pd was the same as Ld and was set to 3 µm, 5 µm, 7 µm and 9 µm. According to the equations in [8], an overlap of 46.7 % to 82.2 % was obtained.

Table 3 Surface roughness as a function of Pd and Ld

Pd = Ld [µm]	3	5	7	9
Pulse and line overlap [%]	82.2	70.4	58.6	46.7
Sa [µm]	0.468	0.301	0.394	0.656
Sz [µm]	4.596	2.731	2.992	4.739

Small pulse distances cause the laser pulse to increasingly interact with the ablation area of the previous pulse [9]. This leads to impurities on the textured surface, which increase the statistical roughness [8] and results in the high surface roughness at Pd = 3 µm. The minimum surface roughness was achieved at Pd = Ld =5 µm, as can be seen in Figure 4.

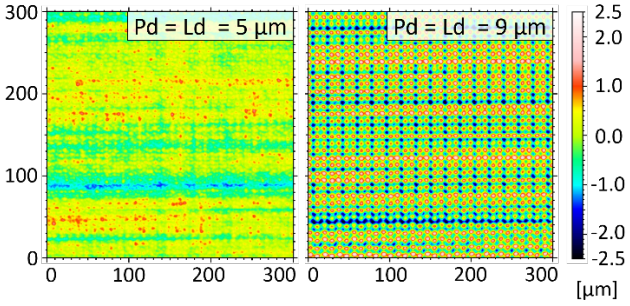

Figure 4. Confocal microscopic surface height map of microstructured hollows with a pulse and line overlap of 70.4 % (left) and 46.7 % (right)

With decreasing overlap, periodic patterns increasingly occur in the same size as the pulse and line distance. These lead to a rise in roughness due to the higher kinematic roughness [8] component. An overlap of 70.4 % offers the best compromise between technical cleanliness and surface quality.

4.3. Removal efficiency

Efficient production of the riblets is essential for subsequent industrial implementation. One quantity for the description of an efficient ablation process is the removal rate or energy specific volume $\Delta V/\Delta E$ [10]. Further, it is important to maintain a smooth surface while keeping the ablated volume per time high. The results are summarized in Figure 5 showing removal efficiency and arithmetic mean roughness versus peak fluence.

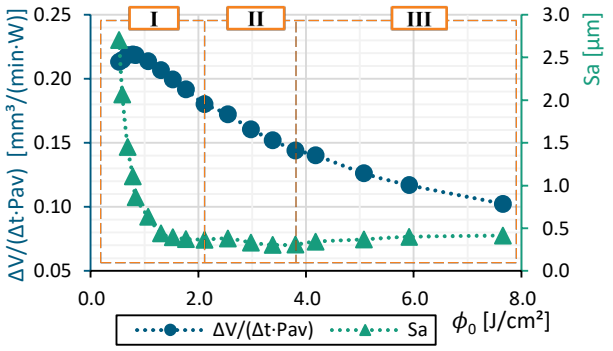

Figure 5. Energy specific volume ΔV/(Δt·Pav) and arithmetical mean height Sa as a function of peak fluence ϕ_0

The course of the removal efficiency as a function of the peak fluence can be divided into three areas. In area I, the removal efficiency is highest. This means that most of the energy is used to ablate the material and only a small amount of energy generates heat or other undesirable effects. Consequently, the best roughness should be machined in area I and only small burr and spatter should be present. However, the roughness of this material increases significantly at peak fluences of less than 2.1 J/cm². This is caused by inclusion induced cones (IIC), which can be seen in the SEM images in Figure 6. IIC appear because the threshold fluence is not reached for the material inclusions and cones remain under the inclusions due to shadowing [11].

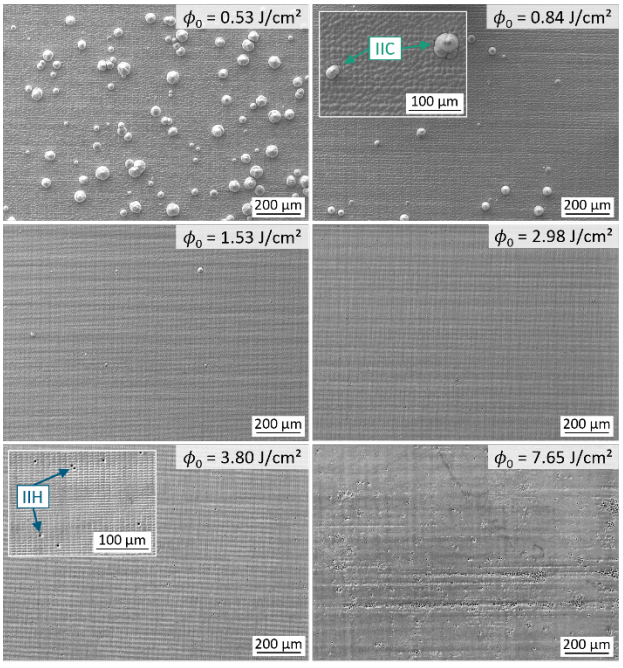

Figure 6. SEM micrograph of the bottom surface of 70 µm deep hollows depending on the of peak fluence ϕ_0

In area II and III the ablation process itself becomes less energetically efficient for higher peak fluences (ΔV/ΔE decreases). At the same time, the surface roughness decreases. At peak fluences of 2.1 J/cm² to 5 J/cm², surface roughness of Sa ~ 0.3 µm is achieved. From 2 J/cm², holes with a size of a few µm (approx. 2-3 µm) can be recognized. The number of holes increases with rising peak fluence. A visual evaluation of the

surfaces under the SEM shows a poorer surface quality for peak fluences greater 3.8 J/cm².

This results from the growing number of micro-holes, which increasingly fissure the surface. One possible explanation for this are material inclusions, as is the case with IIC. The material inclusions in case of the holes have a locally lower threshold fluence than the rest of the material. Consequently, this leads to increased ablation at these positions and thus to micro-holes. In the following, this will be referred to as inclusion induced holes (IIH). IIH are difficult to resolve in roughness measurements, so that the roughness values for peak fluences of 3.8 J/cm² to 5 J/cm² are comparably low. However, the number of IIH increase steadily. For peak fluences greater 5 J/cm² the surface becomes so fissured due to the high pulse energy that the roughness values increase.

The optimum process window (area II) is between 2.1 J/cm² - 3.8 J/cm². The fluence is high enough to avoid IIC and low enough to minimize the number of IIH. A peak fluence of 2.98 J/cm² was selected for riblet machining.

4.4. Scanning strategy

In order to evaluate the previous results, V-grooves were manufactured according to the size specified in section 2. Thereby, different scan strategies were also tested to achieve the sharpest possible tips. Figure 7 shows the results of scan lines with a hatching angle per layer of δ = 37° and δ = 73° to avoid unwanted patterns as well as parallel scan lines to the riblets (δ = 0°) to increase surface structuring productivity.

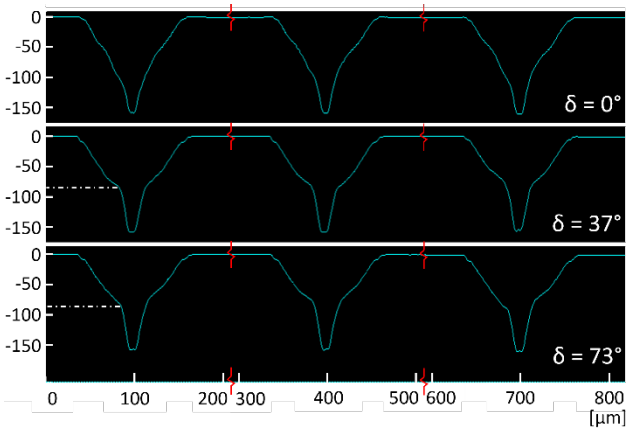

Figure 7. Profile average of 200 lines depending on the scanning strategie with different hatching angles δ

The parallel scan lines showed clear advantages both in terms of geometry and production time. The geometry is characterized by homogeneous flanks and shows the sharpest tip in the base. This is due to the fact that only one line is scanned at the bottom of the V-groove, whose width is determined by the focus diameter. The process time for a test field of 2 x 2 mm² was 140 s.

In comparison, the tip radius is slightly larger when scanning with hatching angle. Due to the angular offset, the scan lines do not run parallel to the groove but are generated at an angle to the groove. The line length determines the size of the tip radius. The length of the scan line is close to 0 µm, but the ExcelliScan moves along this line with acceleration and deceleration distances, whereby the laser on and off delays determine the real line length. The same effect also occurs at the start of the groove, whereby the groove width is approx. 3 µm wider compared to hatching angle δ = 0°. The figure also shows that the scanning strategy with angular offset leads to a significant reduction in the flank angle from half the structure depth. In addition, considerably more scan lines are required to structure the groove with the angular offset strategy. Each of these scan lines also has an acceleration and deceleration section where the laser is off. Furthermore, additional jumps are necessary where otherwise the laser would only execute one line through the groove with parallel processing. This leads to an increase in process time by a factor of 2.2, as the laser is switched off for much longer while the scanner must perform movements.

The effect of the hatching angle on surface roughness was estimated, as well. The hatching angle δ = 37° had the lowest impact on surface roughness (Sa = 0.21 µm) followed by δ = 73° (Sa = 0.23 µm). In case of a hatching angle of δ = 0° the surface roughness was slightly higher (Sa = 0.28 µm). Due to the clear advantages in geometry and production time, with only slightly higher impact on surface roughness, a hatching angle of δ = 0° was chosen for the subsequent experiments.

5. Conclusion

Riblet technology enables the optimization of drag reduction but requires precise design and machining. The simulation was used to design the structure and showed an increase in relative efficiency exceeding 2 % in the operating point. Finally, the suitability of the developed laser process was demonstrated on surface structuring of the designed riblets (see Figure 8).

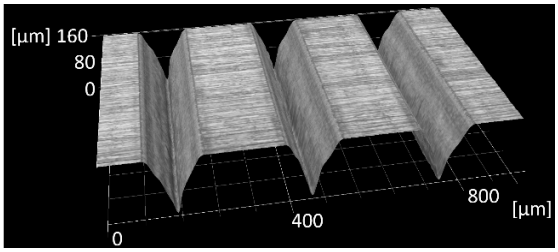

Figure 8. V-grooves of riblet design (s = 300 µm, h = 150 µm, α = 40°) laser structured using f_{rep} = 200 kHz, τ = 0.35 ps, ϕ_0 = 2.98 J/cm², v_{Mark} = 1 m/s, Ld = Pd = 5 µm

The parallel scan lines showed clear advantages both in terms of geometry and production time by slightly higher surface roughness. Femtosecond laser pulses lead to an increased removal rate and resulting in shorter process time. A pulse and line overlap of 70.4 % offers the best compromise between technical cleanliness and surface quality. The optimum process window in case of removal efficiency is between 2.1 J/cm² - 3.8 J/cm². The fluence is high enough to avoid IIC and low enough to minimize the number of IIH.

In further experiments, the moldability and moulding quality of the riblets using injection moulding will be examined. As part of this, the riblet impact will be conducted in a fan pressure chamber and compared to the simulation.

Acknowledgements

Funded by the European Union.

Views and opinions expressed are however those of the author(s) only and do not necessarily reflect those of the European Union. Neither the European Union nor the granting authority can be held responsible for them.

Funded by the European Union

References

[1] Bechert D W et al. 1997 *J. Fl. Mech.* **338** 59
[2] Mayoral R G et al. 2011 *Phil. Trans. R. Soc. A* **369** 1412
[3] Leitl P et al. 2019 *AIAA* 1625
[4] ZIEHL-ABEGG SE 01/09/2025 https://www.ziehl-abegg.com/en-gb/detail/FE3owlet/FG063-SDF.CI.V5P2/188806
[5] Kirchofer M et al. 2023 *Energies* **16** 7864
[6] VDI 3400 Standard 1975
[7] Breitling D et al. 2004 *Proc. SPIE* **5339** 49
[8] Wieland F et al. 2024 *Adv. Eng. Mater.* **26** 2301534
[9] König J et al. 2005 *Opt Express* **26** 10597
[10] Förster D et al. 2021 *Materials* **14** 3331
[11] Villerius V et al. 2019 *J. Mach. T. Manu.* **138** 27